

Supplementary Information for

High-Intensity Focused Ultrasound-Induced Mechanochemical Transduction in Synthetic Elastomers

Gun Kim, Vivian M. Lau, Abigail J. Halmes, Michael L. Oelze, Jeffrey S. Moore, and
King C. Li

Jeffrey S. Moore and King C. Li

Email: jsmoore@illinois.edu; and kingli@illinois.edu

This PDF file includes:

Materials and Methods
Figs. S1 to S7
Tables S1 to S2
Captions for movies S1 to S5
References for SI reference citations

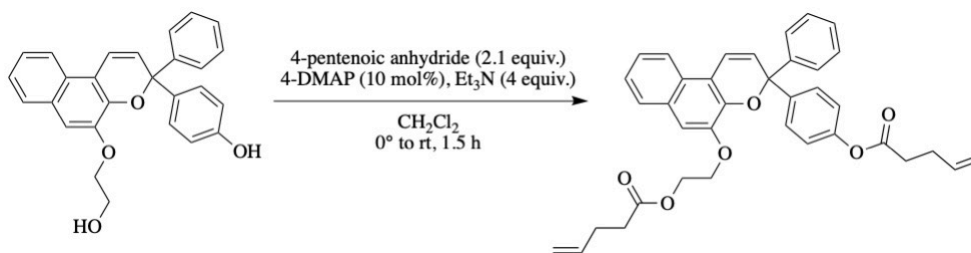
Other supplementary materials for this manuscript include the following:

Movies S1 to S5
NMR Spectra

SI Materials and Methods

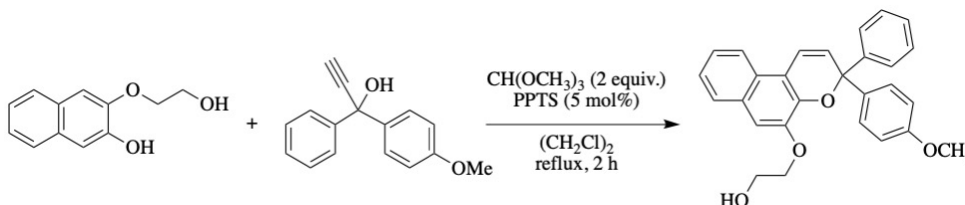
General synthetic methods. All reactions were carried out in oven- or flame-dried glassware, under an atmosphere of dry N₂ unless otherwise indicated. Organic reagents were purchased from Sigma-Aldrich, Fisher Scientific or Acros Organics and used as received. Solvents were purchased as anhydrous grade or dried by passing through an activated alumina column on an Innovative Technology PureSolv solvent purification system. Thin layer chromatography was performed with silica gel-coated aluminum plates (Fluka, with fluorescent indicator) and visualized under UV light or with iodine staining. Flash chromatography was performed with 230-400 mesh silica gel (Silicycle SiliaFlash P60) or using a Biotage Isolera system with SiliaSep Flash cartridges. Routine NMR spectra were obtained on Varian spectrometers (500 MHz Inova). ¹H and ¹³C spectra were referenced to residual solvent signal relative to trimethylsilane. High resolution mass spectrometry was performed on a Waters Q-ToF Ultima using electrospray ionization. The Q-ToF Ultima mass spectrometer was purchased in part with a grant from the National Science Foundation, Division of Biological Infrastructure (DBI-0100085). Previously reported mechanophores were synthesized according to the literature: NP was prepared as previously described (1) and recrystallized from chloroform/ethanol before use. Dioxetane was prepared as previously described (2). A Bruker D8 Venture Duo diffractometer using a Cu source was used to collect X-ray diffraction data on NP single crystals by Dr. Toby Woods in the George L. Clark X-ray Facility. See Table S1 for structure refinement details (CCDC Number: 1890871).

Synthesis of NP.



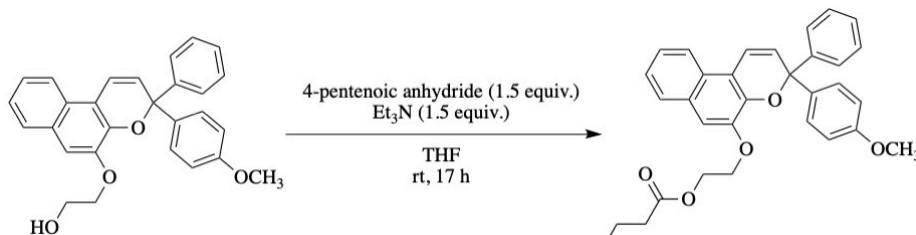
NP was prepared as previously described (1) and recrystallized from chloroform/ethanol before use. NMR characterization matched the previous report, and the structure was further confirmed by x-ray crystallography (Fig. S6 with corresponding information in Table S1).

Synthesis of monofunctional control naphthopyran (NP-control).



A flame-dried 100 mL round-bottom flask was charged with 3-(2-hydroxyethoxy) naphthalene-2-ol (743 mg, 3.64 mmol), 1-(4-methoxyphenyl)-1-phenylprop-2-yn-1-ol (953 mg, 4.0 mmol), and pyridinium p-toluenesulfonate (46.0 mg, 0.182 mmol). Dichloroethane (20 mL) was added via syringe followed by trimethylorthoformate (773 mg, 797 μ L, 7.28 mmol), and the homogeneous

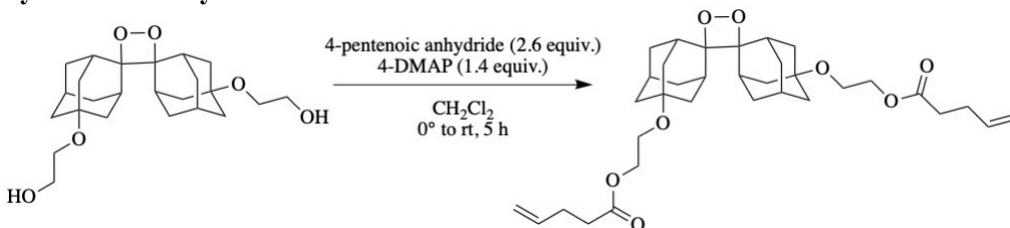
mixture was stirred at reflux for 2 h. After cooling to room temperature, the solvent was removed by evaporation under reduced pressure. Purification of the crude product by column chromatography (SiO₂, 15–50% EtOAc/hexanes) yielded the hydroxy-terminated naphthopyran as a red foam (1.02 g, 2.40 mmol, 66% yield). ¹H NMR (500 MHz, Acetone-d₆) δ: 3.72 (s, 3H), 4.01 (q, *J* = 5.1 Hz, 2H), 4.06 (bs, 1H), 4.27 (t, *J* = 9.9 Hz, 2H), 6.55 (d, *J* = 9.9 Hz, 1H), 6.83–



6.86 (m, 2H), 7.23 (tt, *J* = 7.4, 1.6 Hz, 1H), 7.28–7.35 (m, 5H), 7.43 (d, *J* = 10.0 Hz, 1H), 7.49–7.52 (m, 2H), 7.60 (dt, *J* = 8.4, 1.6 Hz, 2H), 7.69 (dd, *J* = 8.2, 1.0 Hz, 1H), 7.96 (d, *J* = 8.2 Hz, 1H). ¹³C NMR (125 MHz, Acetone-d₆) δ: 55.4, 61.3, 71.4, 82.8, 110.1, 114.1, 116.6, 120.4, 122.0, 125.0, 125.2, 125.9, 127.3, 127.98, 128.04, 128.8, 128.9, 130.1, 130.5, 137.7, 143.4, 146.1, 149.2, 159.9. HRMS (ESI): [M+H⁺] calculated *m/z* = 425.1747 for C₂₈H₂₅O₄⁺, found 425.1773.

The hydroxyl-terminated naphthopyran (510 mg, 1.20 mmol) and 4-(dimethylamino) pyridine (49.0 mg, 0.4 mmol) were charged to a flame-dried 20 mL septum-capped vial. THF (15 mL) was added via syringe, followed by pentenoic anhydride (328 mg, 1.80 mmol) and triethylamine (153 mg, 210 μL, 1.80 mmol). The reaction was stirred for 17 h at room temperature, and then quenched by the addition of 1 mL of MeOH. After evaporation of solvent under reduced pressure, the crude product was purified by column chromatography (SiO₂, 0–30% EtOAc/hexanes) to give the monofunctional control naphthopyran as an orange gel, which solidified on standing (463 mg, 0.915 mmol, 76% yield). ¹H NMR (500 MHz, Acetone-d₆) δ: 2.35 (q, *J* = 6.4 Hz, 2H), 2.46 (t, *J* = 7.1 Hz, 2H), 3.74 (s, 3H), 4.40–4.44 (m, 2H), 4.54–4.57 (m, 2H), 4.91–4.93 (m, 1H), 5.00–5.05 (m, 1H), 5.78–5.8 (m, 1H), 6.60 (d, *J* = 9.9 Hz, 1H), 6.84–6.89 (m, 2H), 7.22–7.25 (m, 1H), 7.29–7.39 (m, 5H), 7.45 (d, *J* = 9.9 Hz, 1H), 7.49–7.54 (m, 2H), 7.59–7.64 (m, 2H), 7.70 (d, *J* = 8.1 Hz, 1H), 7.99 (d, *J* = 8.5 Hz, 1H). ¹³C NMR (125 MHz, Acetone-d₆) δ: 29.5, 33.9, 55.4, 63.3, 67.7, 82.7, 110.2, 114.1, 115.7, 116.7, 120.4, 122.0, 125.0, 125.3, 126.0, 127.1, 128.1, 128.8, 120.0, 130.4, 137.7, 143.3, 146.2, 148.7, 159.9, 173.0. HRMS (ESI): [M+H⁺] calculated *m/z* = 507.2166 for C₃₃H₃₀O₅⁺, found 507.2176.

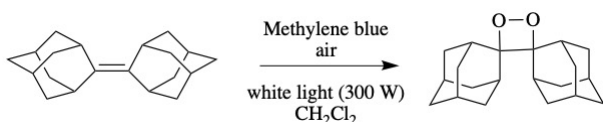
Synthesis of vinyl-terminated dioxetane.



5'/7'-bis(pent-4-enoate-5,5'/7'--dihydroxyethylenoxy)-adamantylideneadamantane 1,2-dioxetane was synthesized as described by Clough *et al* (2). ¹H NMR (500 MHz, CDCl₃) δ 5.94 – 5.72 (m, 2H), 5.17 – 4.92 (m, 4H), 4.23 – 4.09 (m, 2H), 3.59 (dt, *J* = 25.8, 5.0 Hz, 2H), 2.83 (s, 1H), 2.63 (s, 1H), 2.54 – 1.02 (m, 7H). ¹³C NMR (125 MHz, CDCl₃) δ 178.35, 173.21, 136.77, 136.48, 132.24, 115.74, 115.58, 94.02, 72.64, 72.52, 71.72, 71.66, 71.28, 71.10, 64.46, 64.35, 64.26, 64.19, 64.08, 59.21, 58.65, 58.43, 46.86, 42.53, 41.47, 41.22, 41.09, 40.36, 38.56, 38.46, 38.38,

36.23, 36.08, 34.14, 34.10, 33.72, 33.57, 33.56, 33.46, 33.32, 31.67, 30.89, 29.64, 28.90, 28.85, 28.63, 21.04. **HRMS (ESI):** $[M+H]^+$ calculated $m/z = 585.3422$ for $C_{34}H_{49}O_8^+$, found 585.3411.

Synthesis of non-functionalized dioxetane control.



Synthesis of adamantylideneadamantane peroxide was adapted from Clough *et al* (2). 1H NMR (500 MHz, $CDCl_3$) δ 5.30 (s, 6H), 3.48 (q, $J = 7.0$ Hz, 2H), 2.90 (t, $J = 3.1$ Hz, 1H), 2.01 – 1.78 (m, 6H), 1.69 (t, $J = 13.3$ Hz, 3H), 1.58 (s, 1H), 1.33 – 1.17 (m, 5H), 0.91 – 0.81 (m, 2H). ^{13}C NMR (125 MHz, $CDCl_3$) δ 204.17, 95.96, 47.11, 39.78, 39.40, 37.55, 37.51, 37.41, 36.98, 35.30, 34.78, 32.93, 32.04, 31.99, 31.85, 29.84, 28.71, 27.59, 27.38, 27.34, 26.87, 26.67, 22.84, 14.27. **HRMS (ESI):** $[M+Na]^+$ calculated $m/z = 323.1982$ for $C_{20}H_{28}O_2Na^+$, found 323.1988.

HIFU triggering system and beam characteristics. A photograph of the custom HIFU setup for the mechanochemical transduction is provided in Fig. S2A. A function generator (33500B, Keysight Technologies, Santa Rosa, CA) was used to produce a sinusoidal voltage signal with a user-defined signal amplitude. The voltage signal was amplified through a radiofrequency power amplifier (NP Technologies Inc., Newbury Park, CA), a 10 MHz low pass filter and an impedance matching network before being sent to the spherically-focused HIFU transducer (FUS Instruments, Canada) with nominal center frequencies of 550 kHz and 1 MHz, respectively (3). Note that both HIFU transducers have a focal distance of 60 mm and diameter of 75 mm (f-number 0.8). The entire setup was synchronized with the computer programmed to automatically control the input parameters in the function generator and the sonication time. The sonication induced events were recorded using a waterproof digital camera with 1334×750 -pixel resolution placed behind the PDMS films (Fig. 2A, a2).

The spatial pressure distributions of each transducer (550 kHz and 1 MHz) were measured in a tank of degassed water using a fiber-optic hydrophone (10 μ m active element, Precision Acoustics, Dorchester, UK) with a hydrophone step size of 100 μ m in the y-z plane (Fig. S5B). The full width at half maximum (FWHM) beamwidth, B_W and depth of field, Z_F of each transducer were measured to be: 1.2 and 5.9 mm for 1 MHz; and 2.2 and 12.5 mm for 550 kHz, respectively. The output voltage signal measured with the hydrophone was converted to acoustic pressure using the hydrophone sensitivity interpolated from the data provided by the manufacturer (96.00 $mV \cdot MPa^{-1}$ for 550 kHz and 112.04 $mV \cdot MPa^{-1}$ for 1 MHz). The spatial-peak temporal average intensity (I_{SPTA}) was calculated by

$$I_{SPTA} = p^2 \cdot (2 \cdot \rho \cdot c)^{-1} \quad [1]$$

where p is the peak acoustic pressure amplitude, ρ the density of material, and c the speed of sound. It is important to note that the intensity and pressure applied throughout the PDMS samples are slightly less than the estimated values due to reflection at the PDMS surface. The calculated pressure reflection coefficient is approximately -0.186, indicating that the intensity of the transmitted beam into the PDMS samples is decreased by 3.4%, e.g., from I_{SPTA} of $333 \text{ W} \cdot \text{cm}^{-2}$ (in the degassed water) to I_{SPTA} of $322 \text{ W} \cdot \text{cm}^{-2}$ (in the NP-PMDS).

The transmitted ultrasonic beam is hypothesized to trigger the mechanochromic and mechanoluminescent transductions via acoustic radiation force (4):

$$F = 2 \cdot \alpha \cdot I_{SPTA} \cdot c^{-1} \quad [2]$$

where F is the radiation force (force per unit volume, $\text{kg} \cdot \text{s}^{-2} \cdot \text{m}^{-2}$) applied along the longitudinal direction, α the absorption coefficient of the material (m^{-1}).

Due to the negligible contribution of scattering to attenuation in PDMS samples, the radiation force was estimated using the measured attenuation coefficient, a (Table S2). For instance, with the consideration of the reflected waveform at the surface (18.6%), the calculated volumetric radiation force from the acoustic pressure of 3.2 MPa is approximately $8.46 \text{ kg}\cdot\text{s}^{-2}\cdot\text{cm}^{-2}$ for 550 kHz and $10.8 \text{ kg}\cdot\text{s}^{-2}\cdot\text{cm}^{-2}$ for 1 MHz, respectively.

RGB Analysis. Among many methods available for performing image analysis, we employed Image Pro Plus software (Media Cybernetics, Rockville, MD) to analyze the mechanophore-induced color change. The recorded video clips (Movie S1 to S5) with a waterproof digital camera were first reconstructed with a frame rate of 30 frames per second (fps). Then, the region of interest (ROI) set to be smaller than the colored area was applied through all frames. The ratio of the ROI to the colored area was fixed to less than 0.5 to improve the intensity, and SNR of three RGB peaks. The time-lapse frames shown in Fig. 2 and Fig. 3 were chosen based on the lowest value of the blue channel, and using this value, comparison of each RGB channels (0 to 255) was conducted. In a similar way, the light intensity analysis was also achieved (Fig. 5).

Acoustic properties of PDMS materials. To quantify the acoustic properties of the prepared NP-PDMS samples, speed of sound and attenuation were estimated using the methods introduced in (5). An Olympus 5800 pulser/receiver operated in pulse-echo mode with a pulse repetition frequency of 1 kHz, and the generated signal was fed to a single-element focused transducer (550 kHz or 1 MHz, f-number 3) aligned perpendicular to the sample in a degassed water bath (21 ± 2 °C). Each transducer was positioned in front of the sample, respectively, at a distance of 5.7 cm, which is the nominal focal distance (Fig. S7). The reflected pulses from the top and bottom surfaces of a 5 mm thick flat NP-PDMS sample were averaged at least 100 times to increase signal-to-noise ratio (SNR) and recorded into a computer (Fig. S2B). Based on the time-of-flight (TOF) method, the speed of sound, c of the NP-PDMS was estimated by dividing the sample thickness by the time difference between the measured reflected signals. The averaged speed of sound in NP-PDMS was approximately $1170 \text{ m}\cdot\text{s}^{-1}$. This estimated value is comparable to that of Sylgard 184 reported in the literature (6), suggesting that the mechanophore itself does not significantly affect the acoustic properties of PDMS. Using the measured density, ρ of the PDMS sample ($= 870 \text{ kg}\cdot\text{m}^{-3}$), the acoustic impedance, $Z_o (= \rho \cdot c)$ was calculated to be $1.02 \text{ MRayl} (= \text{MPa}\cdot\text{s}\cdot\text{m}^{-1})$. The attenuation coefficient, a (dB/cm) was estimated via a pulse-echo insertion loss method (5):

$$a(f) = 10 \cdot (2d)^{-1} \cdot \log_{10} (P_r(f) \cdot P_s(f)^{-1}). \quad [3]$$

where $P_r(f)$ and $P_s(f)^{-1}$ are the power spectrum of the reflected waveform from a reflector with and without the NP-PDMS samples, and d is the sample thickness.

The spectral log difference in Equation (1) has a linear trend within the effective bandwidth, which enables the estimation of the attenuation coefficient for each excitation frequency ($1.60 \pm 0.04 \text{ dB}\cdot\text{cm}^{-1}$ for 550 kHz and $2.05 \pm 0.04 \text{ dB}\cdot\text{cm}^{-1}$ for 1 MHz). The measured acoustic and mechanical properties of the NP-PDMS are listed in Table S2.

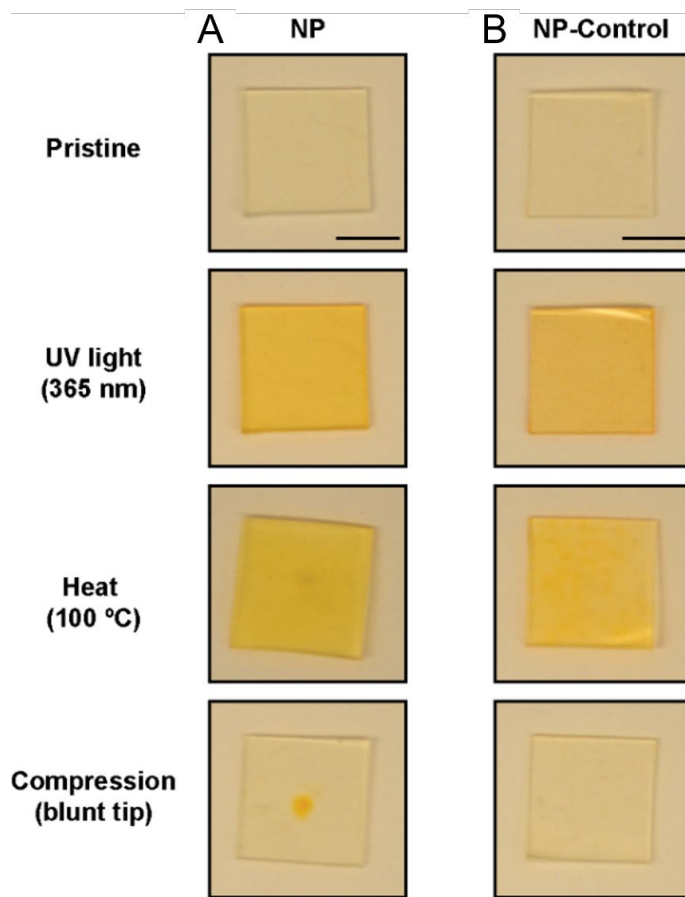


Fig. S1. Photographs of PDMS films covalently functionalized with either NP (A) or NP-control (B) in response to external stimuli. Both NP and NP-control films are photo- and thermochromic; only the NP-containing film is mechanochromic, with localized color change at the site of compression by a blunt-tipped stylus. Scale bar = 5 mm.

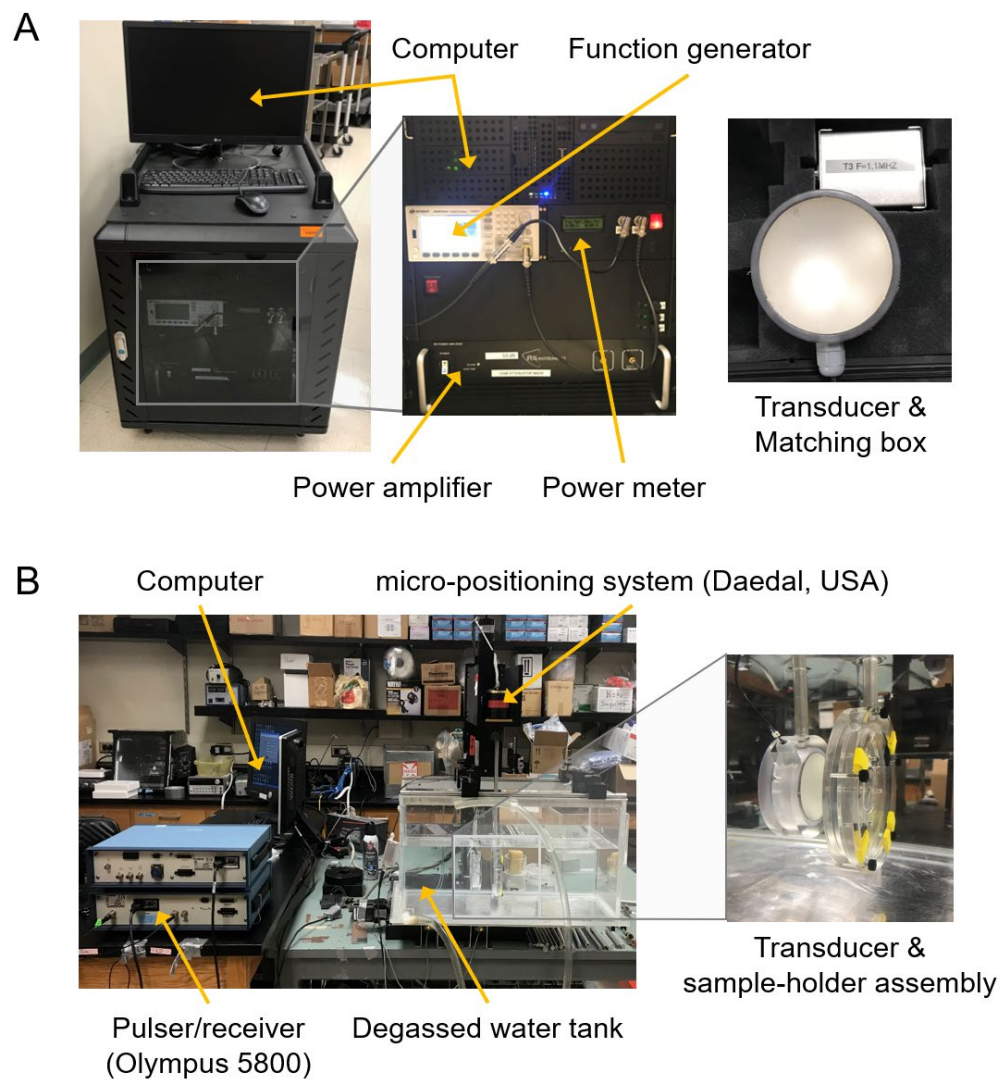


Fig. S2. Photograph of the (A) high-intensity focused ultrasound (HIFU) setup and (B) setup for the spatial control of mechanochemical transduction.

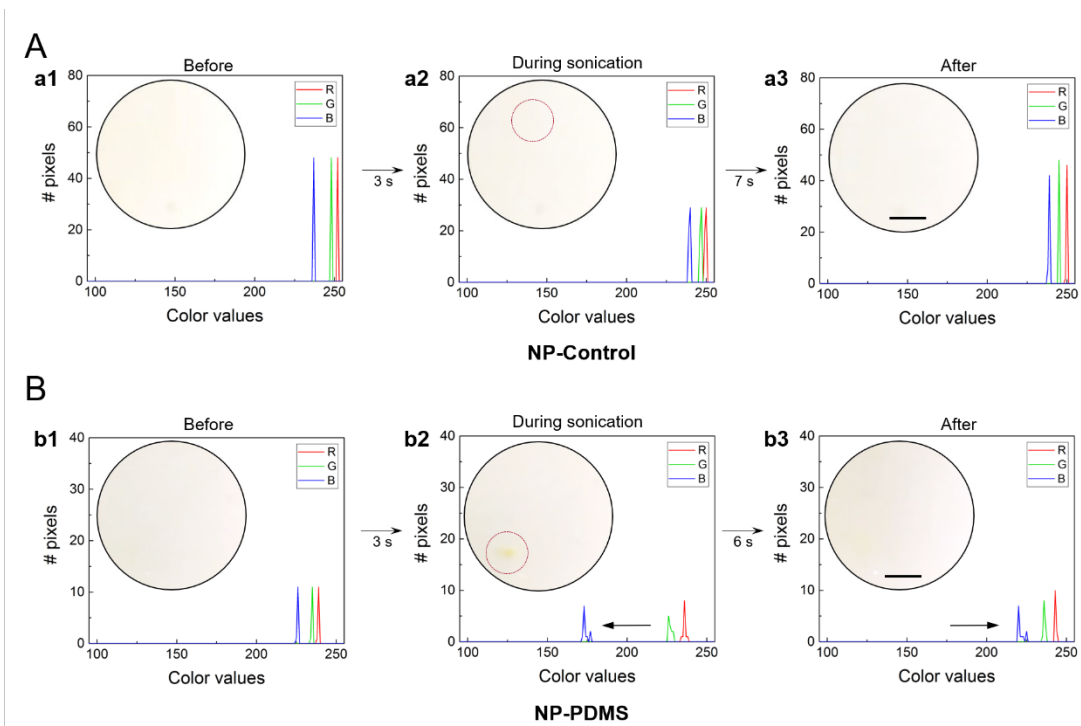


Fig. S3. RGB analysis of mechanochromic response: (A) NP-control; and (B) NP-PDMS. The RGB analysis confirms that the formation of the orange-colored merocyanine species results in significant shift in the blue channel, 226 (before) \rightarrow 174 (during) \rightarrow 221 (after). Scale bar = 2.5 mm.

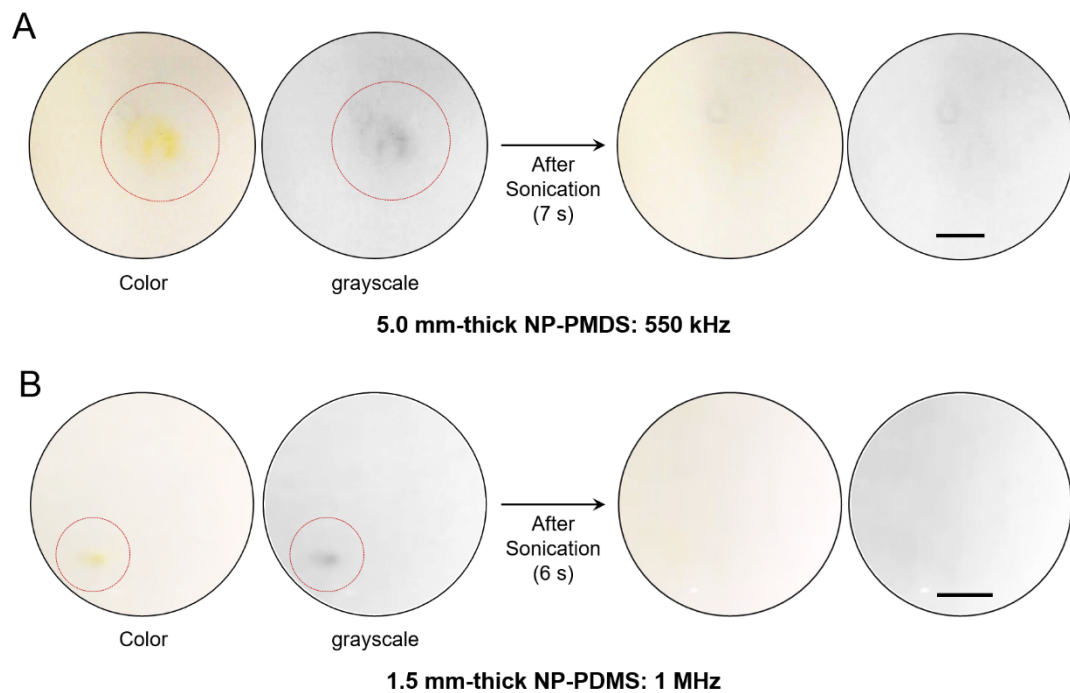


Fig. S4. Activation of naphthopyran mechanophore in color and grayscale images: (A) 5 mm-thick NP-PDMS film with 550 kHz; and (B) 1.5 mm-thick NP-PDMS film with 1 MHz. Grayscale images explicitly shows the activated area and its dependency on the wavelength of the excitation frequency ($\lambda = c/f$). Scale bar = 2.5 mm.

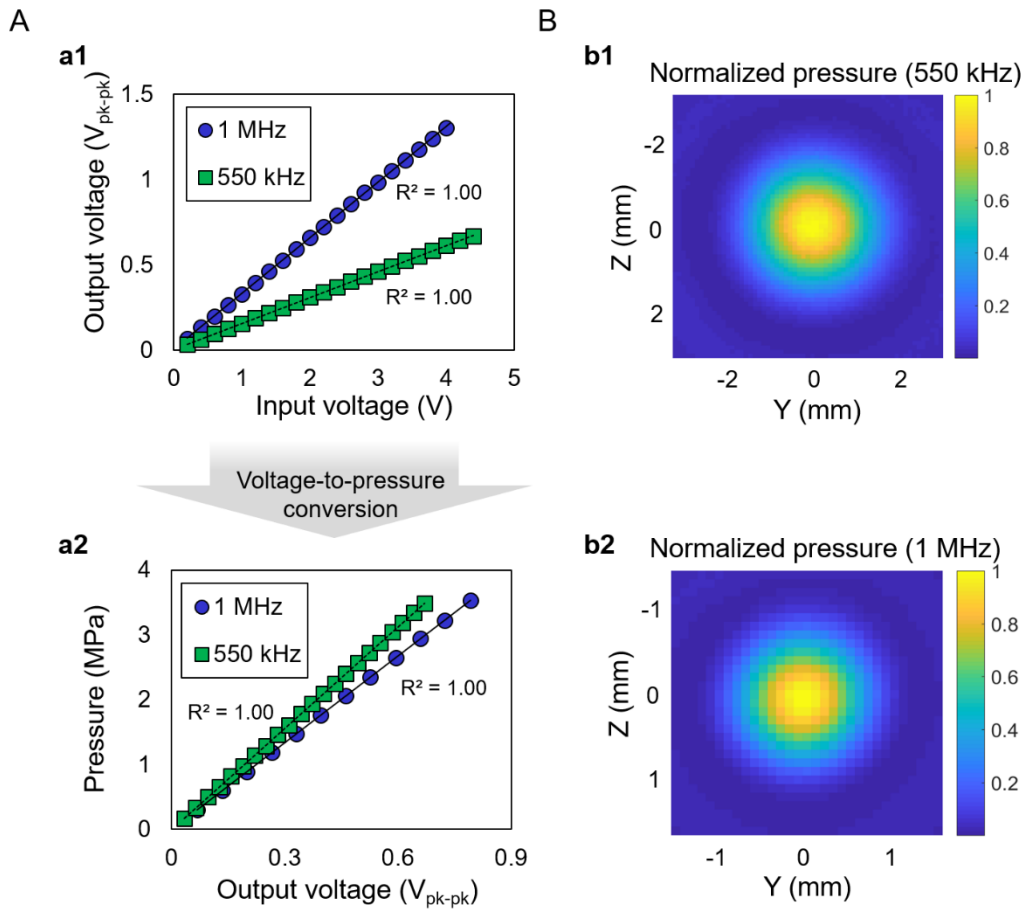


Fig. S5. Calibration of HIFU setup: (A) voltage-to-pressure conversion (the green square for 550 kHz and the blue circle for 1 MHz); and (B) example of the obtained pressure profile (left: electric power = 1.78 W, 550 kHz, and right: electric power = 1.72 W, 1 MHz).

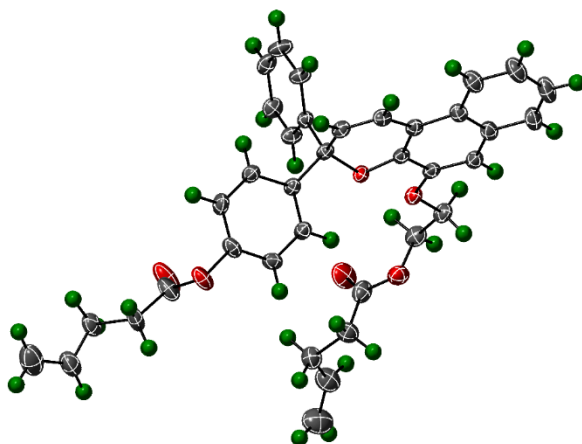


Fig. S6. Molecular structure of the bisvinyl-terminated NP mechanophore refined from single crystal X-ray diffraction data. See Table S1 for refinement details.

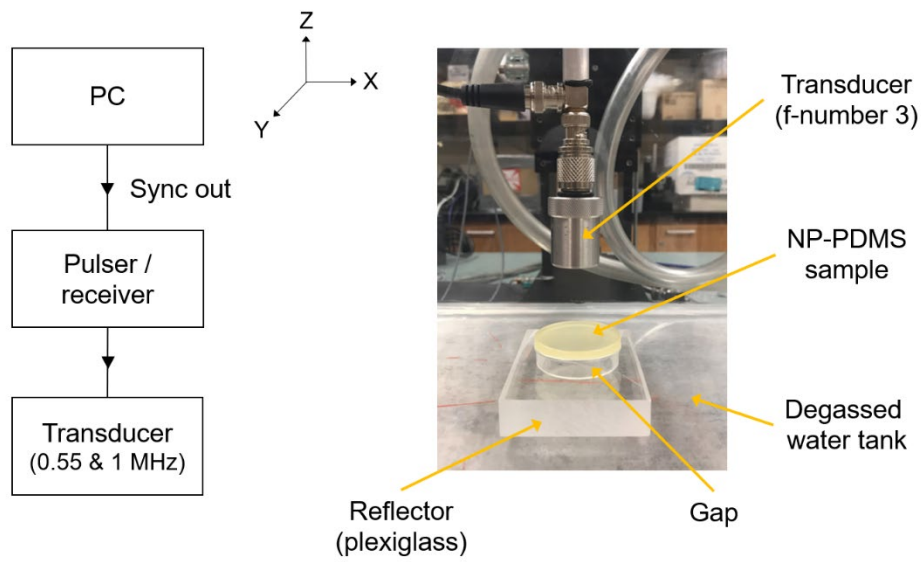


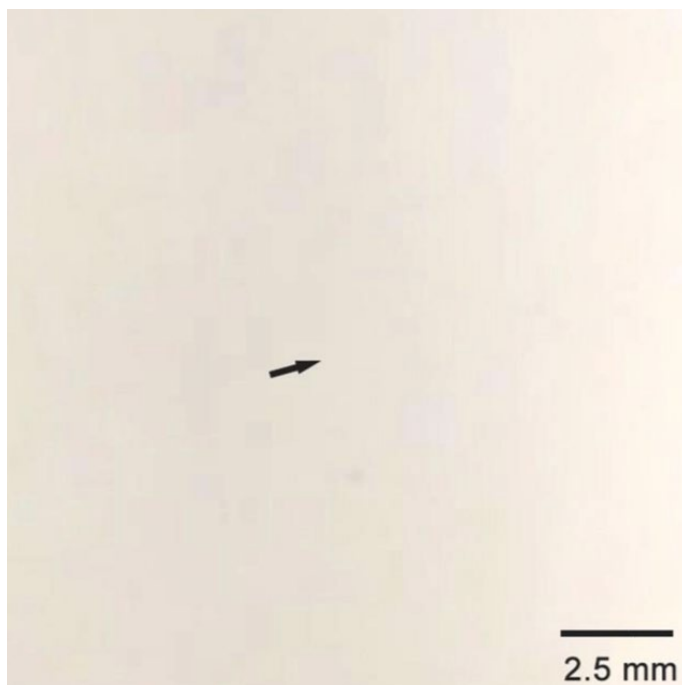
Fig. S7. Speed of sound and attenuation estimation. Attenuation coefficient, a is obtained from the log difference of the power spectrum from a reflector with and without NP-PDMS sample.

Table S1. Structure Refinement Details for the NP Mechanophore

Identification code	dd34nsa	
CCDC Number	1890871	
Empirical formula	C37 H34 O6	
Formula weight	574.64	
Temperature	200(2) K	
Wavelength	1.54178 Å	
Crystal system	Monoclinic	
Space group	P2 ₁	
Unit cell dimensions	a = 12.6780(3) Å	a = 90°
	b = 8.3614(2) Å	b = 105.3502(8)°
	c = 14.8699(4) Å	g = 90°
Volume	1520.06(7) Å ³	
Z	2	
Density (calculated)	1.255 Mg/m ³	
Absorption coefficient	0.681 mm ⁻¹	
F(000)	608	
Crystal size	0.368 x 0.257 x 0.130 mm ³	
Theta range for data collection	3.615 to 68.435°	
Index ranges	-15 ≤ h ≤ 15, -10 ≤ k ≤ 10, -17 ≤ l ≤ 17	
Reflections collected	23941	
Independent reflections	5556 [R(int) = 0.0321]	
Completeness to theta = 67.679°	99.9 %	
Absorption correction	Integration	
Max. and min. transmission	0.9599 and 0.8294	
Refinement method	Full-matrix least-squares on F ²	
Data / restraints / parameters	5556 / 203 / 470	
Goodness-of-fit on F ²	1.064	
Final R indices [I > 2σ(I)]	R1 = 0.0321, wR2 = 0.0785	
R indices (all data)	R1 = 0.0333, wR2 = 0.0796	
Absolute structure parameter	0.39(19)	
Extinction coefficient	0.0224(11)	
Largest diff. peak and hole	0.267 and -0.160 e.Å ⁻³	

Table S2. Acoustic parameters of PDMS with the NP mechanophore

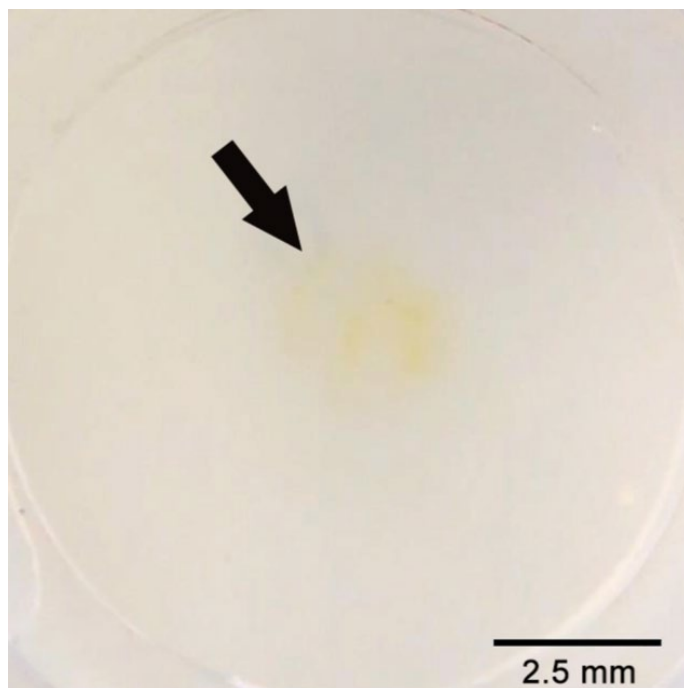
Speed of sound, c ($\text{m}\cdot\text{s}^{-1}$)	1169.3
Acoustic impedance, Z_o ($\text{MPa}\cdot\text{s}\cdot\text{m}^{-1}$)	1.012
Attenuation coefficient, a ($\text{dB}\cdot\text{m}^{-1}$)	160 (550 kHz) & 205 (1 MHz)
Density, ρ ($\text{kg}\cdot\text{m}^{-3}$)	865.8



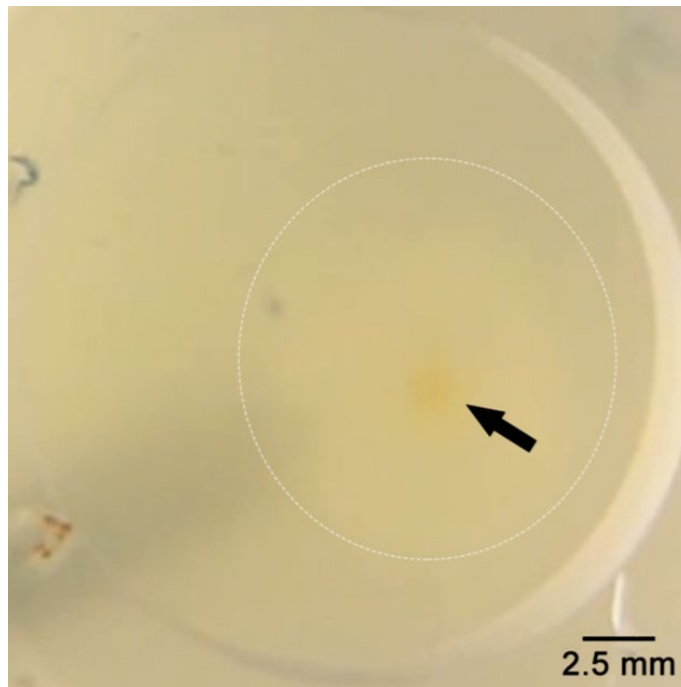
Movie S1. Activation of NP-control in 1.5 mm-thick PDMS. No visible color change demonstrates that the applied 3.2 MPa does not provide sufficient thermal energy to cause NP isomerization. Scale bar = 2.5 mm.



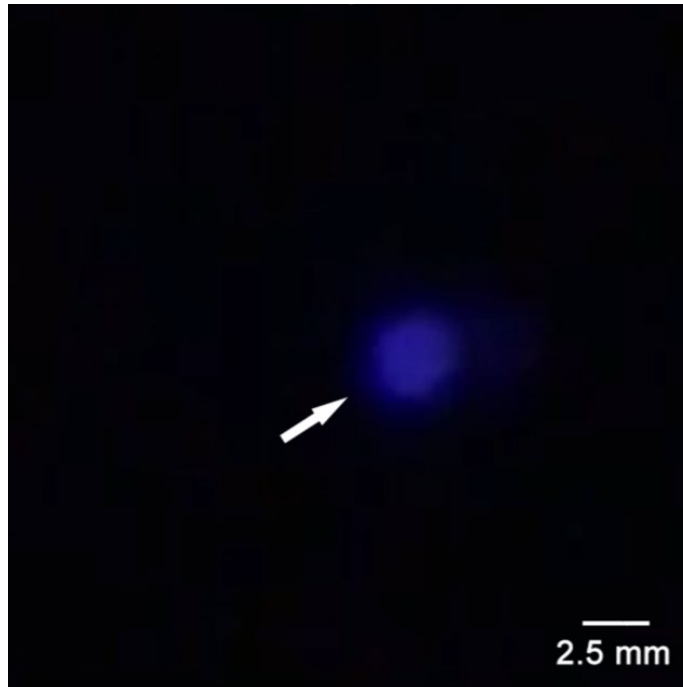
Movie S2. Activation of NP-functionalized mechanophore in 1.5 mm-thick PDMS. The pressure of 3.2 MPa is the maximum value that leads a reversible color change within the localized area while avoiding thermally-induced damage. This shows the importance of the moderate use of acoustic pressure and sonication time for a pure mechanochemical irradiation. Scale bar = 2.5 mm.



Movie S3. Activation of NP-functionalized mechanophore in 5.0 mm-thick PDMS with the pressure of 3.2 MPa. The difference in the dimension of the colored area shows that the mechanophore activation is determined by the beamwidth of the excitation frequency (approximately 2.7 mm for 550 kHz and 1.2 mm for 1 MHz). Scale bar = 2.5 mm.



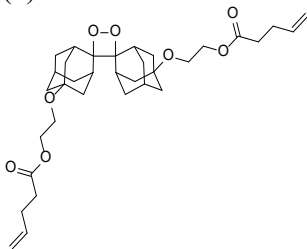
Movie S4. Through-skull activation of hemisphere PDMS. Observation of the reversible color change demonstrates the potential for bio-medical applications such as *in vivo* activation of mechanoluminescence through intervening tissues. Scale bar = 2.5 mm.



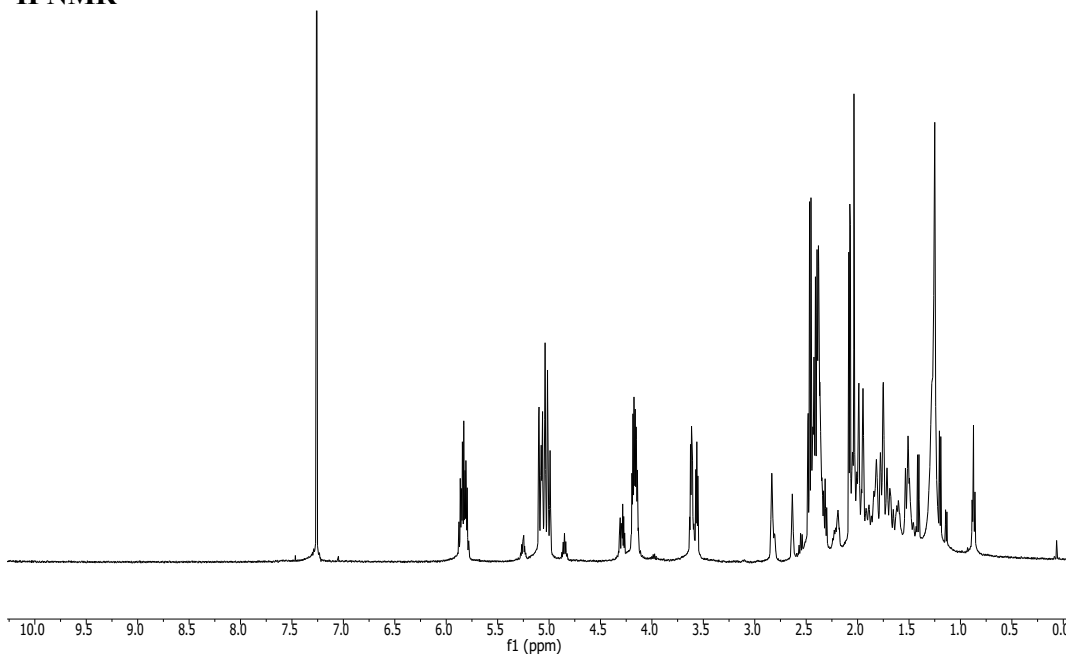
Movie S5. Remote light generation from the mechanoluminescent PDMS. Emission of the blue light shows that integrated with current optogenetic methods, the proposed HIFU can provide a new therapeutic platform, leveraging the advantages of optogenetics research. Scale bar = 2.5 mm.

NMR Spectra

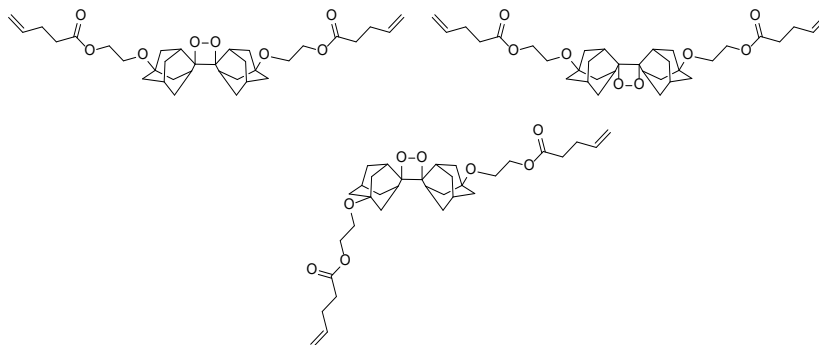
(1)



^1H NMR

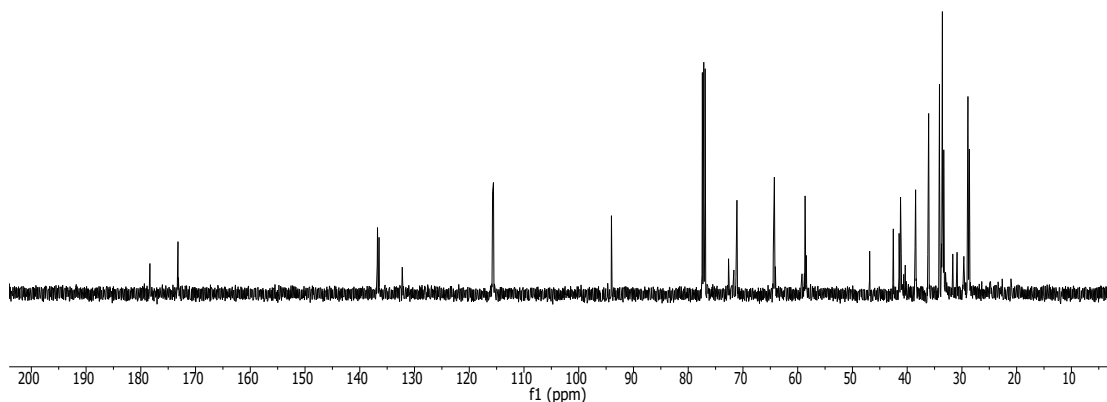


^1H NMR (500 MHz, CDCl_3) spectrum of 5,5'/7'-bis(pent-4-enoate)-5,5'/7'-dihydroxyethylenoxyadamantylideneadamantane 1,2-dioxetane. The reason for the complexity of the spectrum, especially in the high field region is the existence of three constitutional isomers of the compound (Scheme S1).



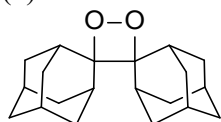
Scheme S1. The three constitutional isomers of the vinyl functionalized dioxetane mechanophore.

¹³C NMR

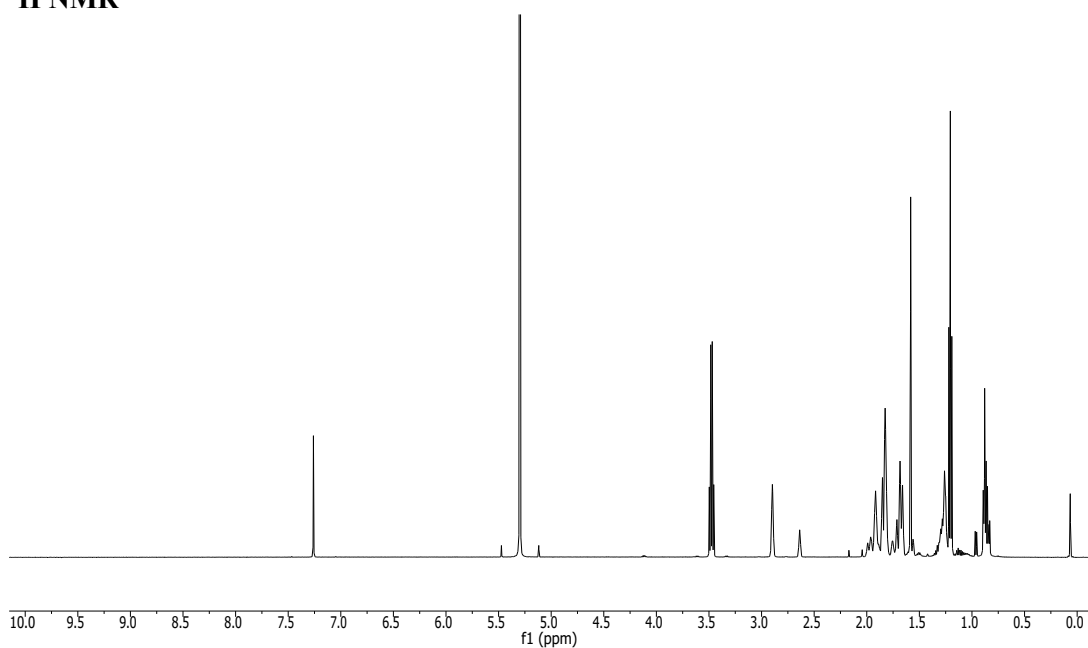


¹³C NMR (125 MHz, CDCl₃) spectrum of 5,5'/7'-bis(pent-4-enoate-5,5'/7'-dihydroxyethylenoxy)adamantylideneadamantane 1,2-dioxetane.

(2)

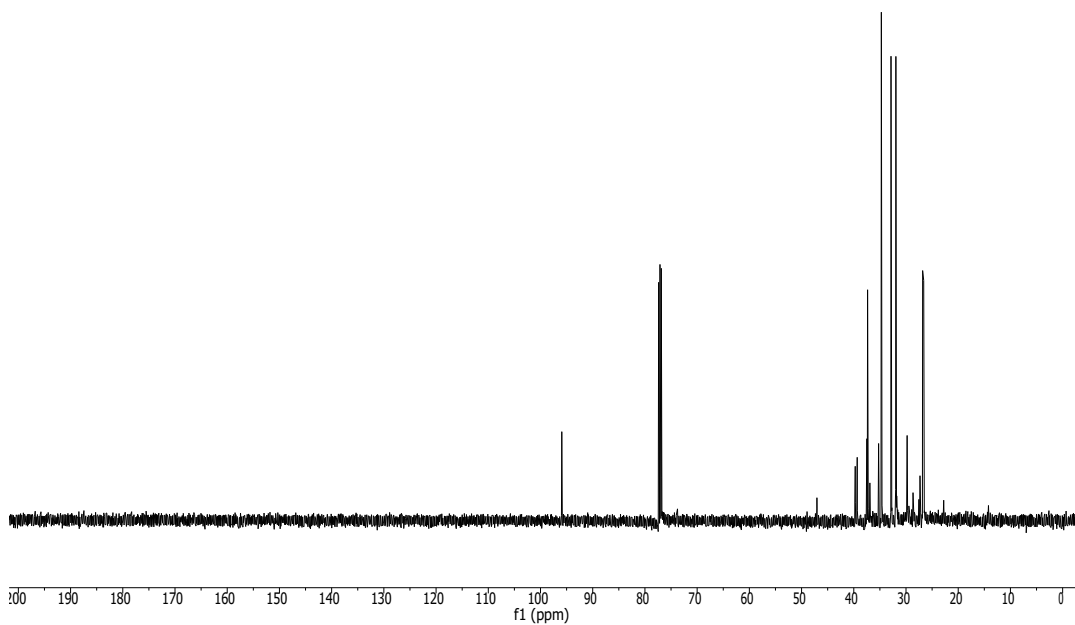


¹H NMR



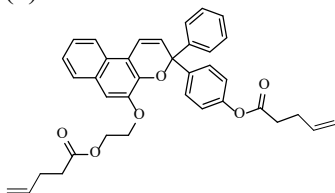
¹H NMR (500 MHz, CDCl₃) spectrum of dioxetane control.

^{13}C NMR

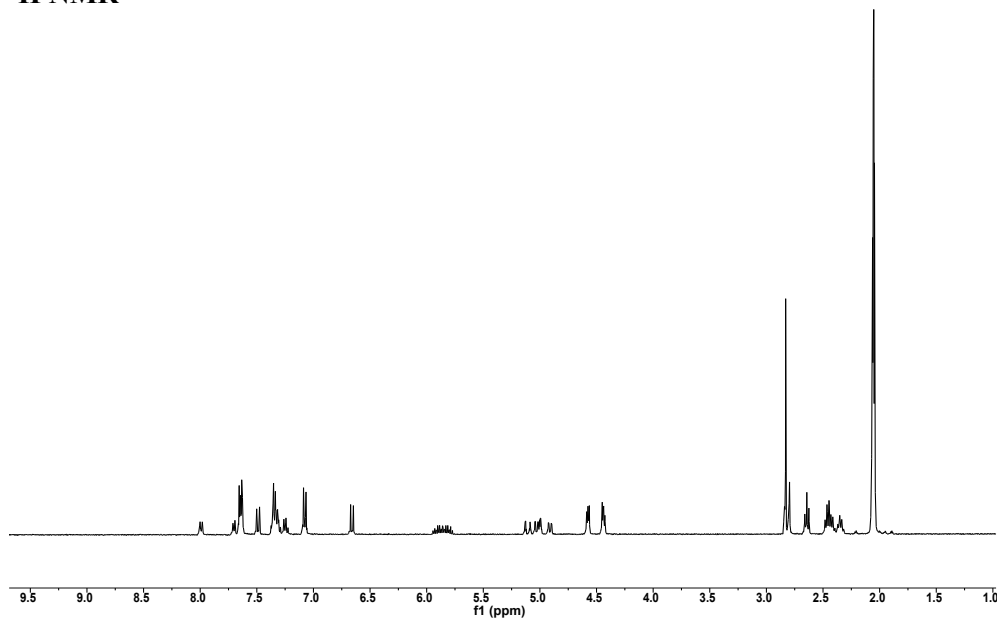


^{13}C NMR (125 MHz, CDCl_3) spectrum of dioxetane control

(3)

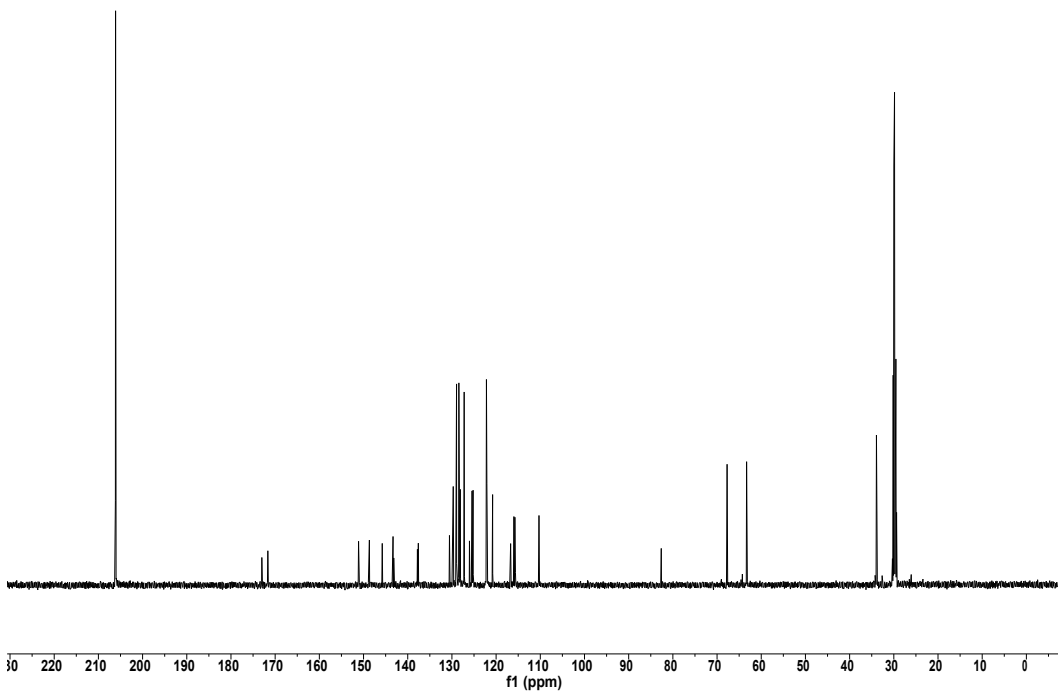


^1H NMR



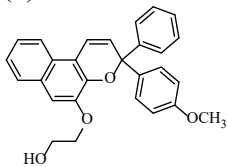
^1H NMR (500 MHz, Acetone-d_6) spectrum of NP.

^{13}C NMR

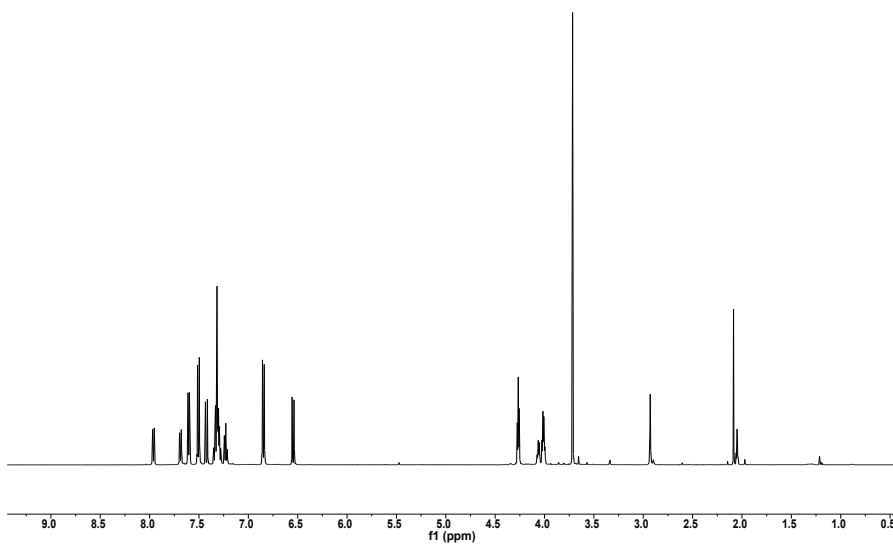


^{13}C NMR (125 MHz, Acetone- d_6) spectrum of NP.

(4)

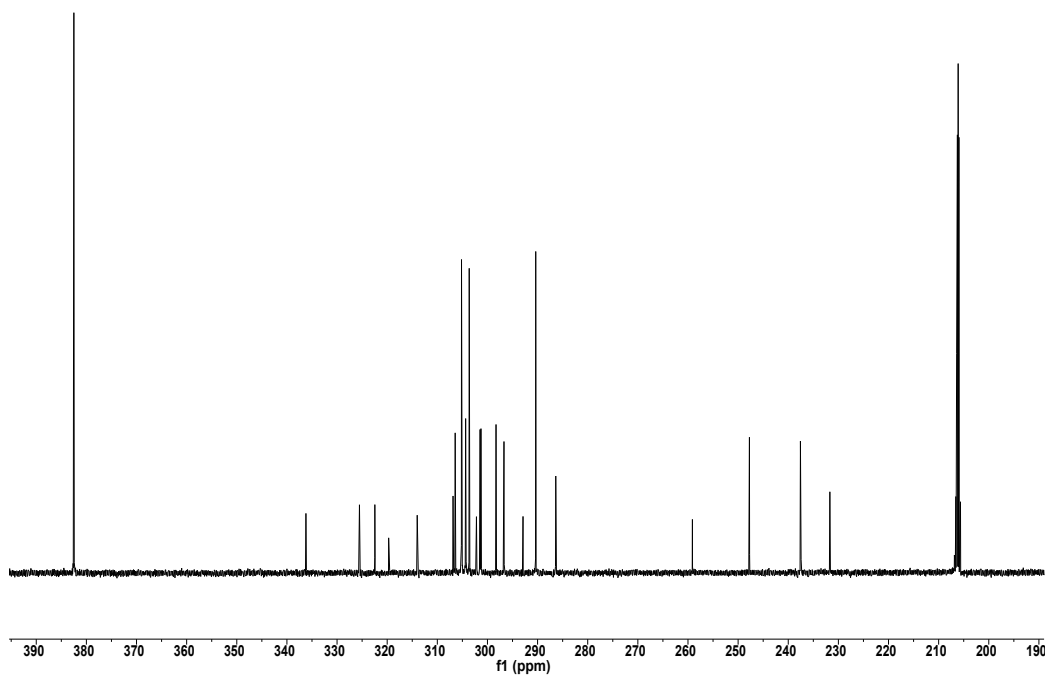


^1H NMR



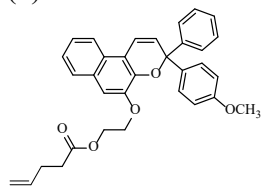
^1H NMR (500 MHz, Acetone- d_6) spectrum of non-functionalized control NP.

¹³C NMR

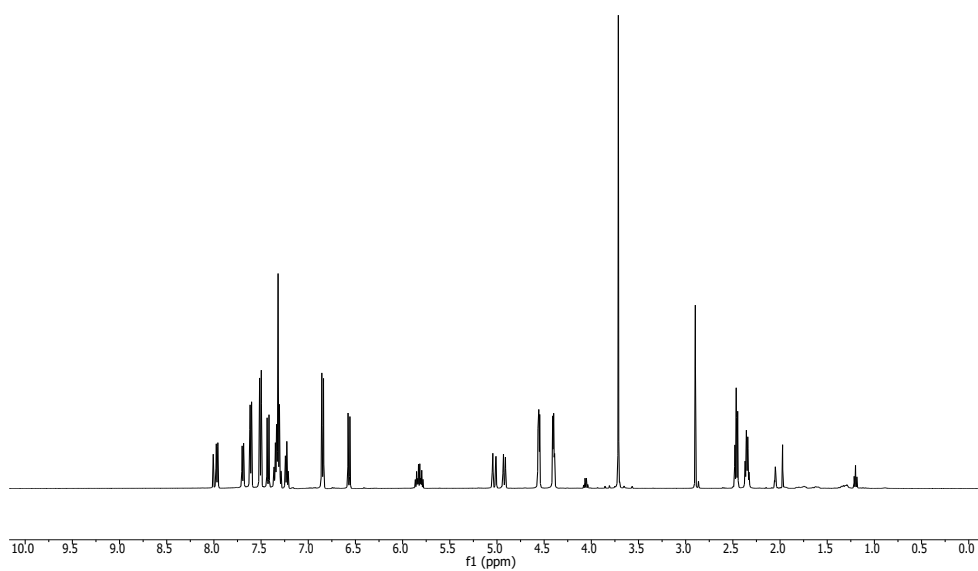


¹³C NMR (125 MHz, Acetone-d₆) spectrum of non-functionalized control NP.

(5)

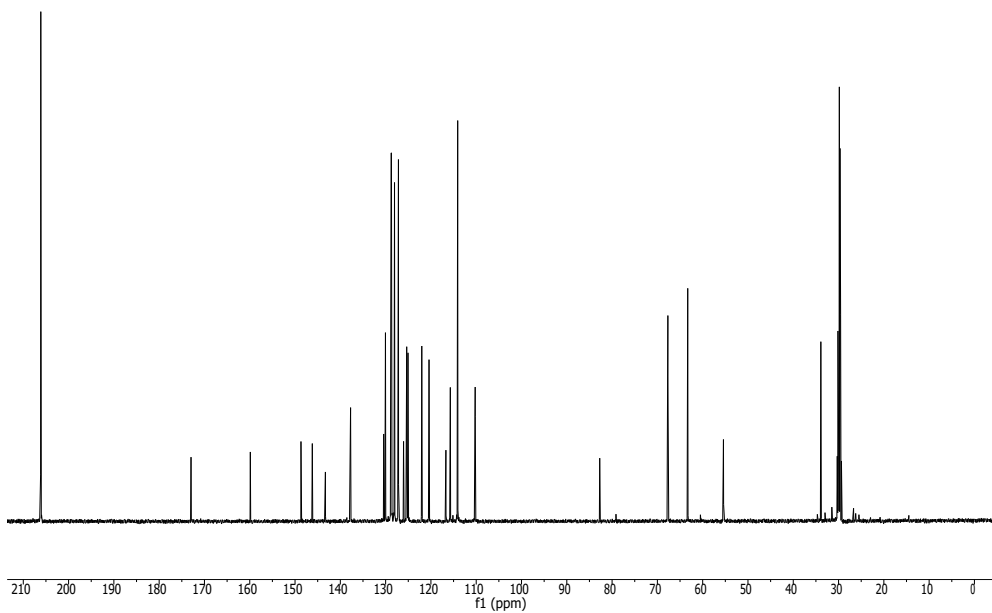


¹H NMR



¹H NMR (500 MHz, Acetone-d₆) spectrum of vinyl terminated control NP.

^{13}C NMR



^{13}C NMR (125 MHz, Acetone- d_6) spectrum of vinyl terminated control NP.

References

1. Robb MJ, et al. (2016) Regioisomer-specific mechanochromism of naphthopyran in polymeric materials. *J Am Chem Soc* 138(38):12328–12331.
2. Clough JM, Creton C, Craig SL, Sijbesma RP (2016) Covalent bond scission in the Mullins effect of a filled elastomer: real-time visualization with mechanoluminescence. *Adv Funct Mater* 26(48):9063–9074.
3. Ellens NPK, et al. (2016) The targeting accuracy of a preclinical MRI-guided focused ultrasound system. *Med Phys* 42(1):430–439.
4. Nightingale K, Soo MS, Nightingale R, Trahey G (2002) Acoustic radiation force impulse imaging: in vivo demonstration of clinical feasibility. *Ultrasound Med Biol* 28(2):227–235.
5. Kemmerer JP, Oelze ML (2012) Ultrasonic assessment of thermal therapy in rat liver. *Ultrasound Med Biol* 38(12):2130–2137.
6. Yuk H, et al. (2017) Hydraulic hydrogel actuators and robots optically and sonically camouflaged in water. *Nat Commun* 8:14230.